CRUK/MRC Oxford Institute for Radiation Oncology

The most likely path of protons in heterogeneous media and its application to proton computed tomography

Mark Brooke[1], Scott Penfold[2,3]

[1] *CRUK/MRC Oxford Institute for Radiation Oncology*
University of Oxford

[2] *Department of Physics*
University of Adelaide

[3] *Department of Medical Physics*
Royal Adelaide Hospital

Presented at Loma Linda University
August 07 2018

mark.brooke@oncology.ox.ac.uk @markdanbrooke

Introduction to proton CT imaging

Stopping power and water equivalent path length

Definition

Stopping power: energy loss of the proton per unit length (MeV/cm);

$$S(E) \equiv -\frac{dE}{dl}. \quad (1)$$

Introduction to proton CT imaging

Stopping power and water equivalent path length

Definition

Stopping power: energy loss of the proton per unit length (MeV/cm);

$$S(E) \equiv -\frac{dE}{dl}. \tag{1}$$

Definition

Water equivalent path length (WEPL): total length of path travelled by a proton in water;

$$\mathrm{WEPL} \equiv \int_{E_{\mathrm{out}}}^{E_{\mathrm{in}}} \frac{1}{S(E)} dE. \tag{2}$$

Introduction to proton CT imaging

Overview

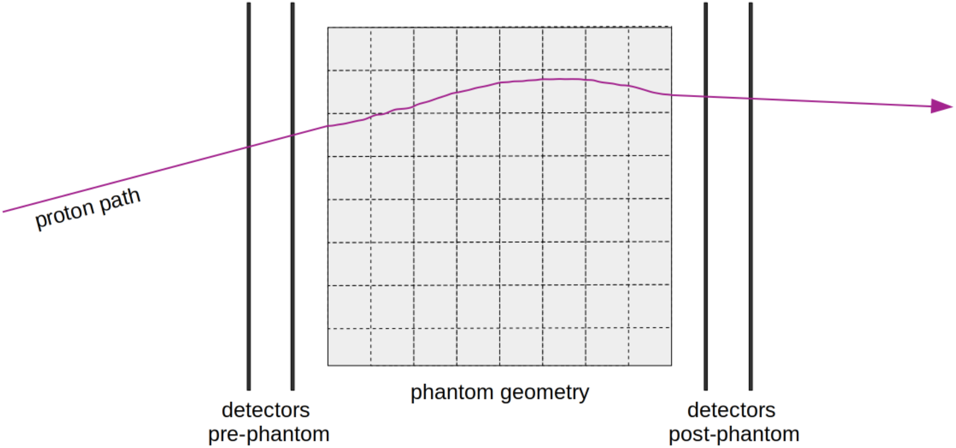

Introduction to proton CT imaging

Overview

- Seek to solve a system of linear equations $A\vec{x} = \vec{b}$

Introduction to proton CT imaging

Overview

- Seek to solve a system of linear equations $A\vec{x} = \vec{b}$
- a_j^i is the path length of the i-th proton through the j-th voxel

Introduction to proton CT imaging

Overview

- Seek to solve a system of linear equations $A\vec{x} = \vec{b}$
- a^i_j is the path length of the i-th proton through the j-th voxel
- b_i is the WEPL of the i-th proton

Introduction to proton CT imaging

Overview

- Seek to solve a system of linear equations $A\vec{x} = \vec{b}$
- a^i_j is the path length of the i-th proton through the j-th voxel
- b_i is the WEPL of the i-th proton
- x_j is the *relative stopping power* (RStP) in the j-th voxel

Introduction to proton CT imaging

Overview

- Seek to solve a system of linear equations $A\vec{x} = \vec{b}$
- a^i_j is the path length of the i-th proton through the j-th voxel
- b_i is the WEPL of the i-th proton
- x_j is the *relative stopping power* (RStP) in the j-th voxel

Introduction to proton CT imaging

Overview

- Seek to solve a system of linear equations $A\vec{x} = \vec{b}$
- a_j^i is the path length of the i-th proton through the j-th voxel
- b_i is the WEPL of the i-th proton
- x_j is the *relative stopping power* (RStP) in the j-th voxel

Definition

Relative stopping power (RStP): the ratio of the stopping power in the material of interest to that in water at the same energy;

$$\mathrm{RStP} \equiv \hat{S}(E) = \frac{S(E)}{S_{\mathrm{w}}(E)}. \tag{3}$$

Introduction to proton CT imaging

Why use protons?

- In clinical practice RStP is estimated by conversion of X-ray CT Hounsfield via an empirically derived calibration curve

Introduction to proton CT imaging

Why use protons?

- In clinical practice RStP is estimated by conversion of X-ray CT Hounsfield via an empirically derived calibration curve
- This approach can lead to errors in stopping power of up to 3% [Smith, 2009; Jiang et al., 2007]

Introduction to proton CT imaging

Why use protons?

- In clinical practice RStP is estimated by conversion of X-ray CT Hounsfield via an empirically derived calibration curve
- This approach can lead to errors in stopping power of up to 3% [Smith, 2009; Jiang et al., 2007]
- pCT is an alternative approach in which RStP of the patient is measured directly with an energetic proton beam

Introduction to proton CT imaging

Why use protons?

- In clinical practice RStP is estimated by conversion of X-ray CT Hounsfield via an empirically derived calibration curve
- This approach can lead to errors in stopping power of up to 3% [Smith, 2009; Jiang et al., 2007]
- pCT is an alternative approach in which RStP of the patient is measured directly with an energetic proton beam
- In iterative pCT reconstruction, one may first assume the imaged object is made purely of water

Introduction to proton CT imaging

Why use protons?

- In clinical practice RStP is estimated by conversion of X-ray CT Hounsfield via an empirically derived calibration curve
- This approach can lead to errors in stopping power of up to 3% [Smith, 2009; Jiang et al., 2007]
- pCT is an alternative approach in which RStP of the patient is measured directly with an energetic proton beam
- In iterative pCT reconstruction, one may first assume the imaged object is made purely of water
- On each successive iteration the internal composition may be updated

Most likely path of protons

Importance

- Protons do not move in straight lines

Most likely path of protons

Importance

- Protons do not move in straight lines
- Multiple Coulomb scattering (MCS) poses a challenge in pCT image reconstruction

Most likely path of protons

Importance

- Protons do not move in straight lines
- Multiple Coulomb scattering (MCS) poses a challenge in pCT image reconstruction
- Assumption of straight line paths is replaced with Bayesian models of the most likely path (MLP) [Williams, 2004; Schulte et al., 2008]

Most likely path of protons
Importance

- Protons do not move in straight lines
- Multiple Coulomb scattering (MCS) poses a challenge in pCT image reconstruction
- Assumption of straight line paths is replaced with Bayesian models of the most likely path (MLP) [Williams, 2004; Schulte et al., 2008]
- MLP is currently calculated under the assumption that the imaged body consists entirely of water

Most likely path of protons
Importance

- Protons do not move in straight lines
- Multiple Coulomb scattering (MCS) poses a challenge in pCT image reconstruction
- Assumption of straight line paths is replaced with Bayesian models of the most likely path (MLP) [Williams, 2004; Schulte et al., 2008]
- MLP is currently calculated under the assumption that the imaged body consists entirely of water
- We present an MLP formalism that takes into account the inhomogeneous composition of the human body

Most likely path of protons

Bayesian formalism

- Matrix-based MLP formula [Schulte et al., 2008]

Most likely path of protons

Bayesian formalism

- Matrix-based MLP formula [Schulte et al., 2008]
- Uses Bayesian probability theory

Most likely path of protons

Bayesian formalism

- Matrix-based MLP formula [Schulte et al., 2008]
- Uses Bayesian probability theory
- Uses entry and exit information to infer most likely trajectory through water

Most likely path of protons
Bayesian formalism

- Matrix-based MLP formula [Schulte et al., 2008]
- Uses Bayesian probability theory
- Uses entry and exit information to infer most likely trajectory through water
- the most likely lateral position t_1 and angular deflection θ_1 at an intermediate depth u_1 are represented by the vector $\mathrm{y}_1 = \begin{pmatrix} t_1 & \theta_1 \end{pmatrix}^{\mathrm{T}}$, given the respective entry and exit conditions, $\mathrm{y}_{\mathrm{in}} = \mathrm{y}_0 = \begin{pmatrix} t_0 & \theta_0 \end{pmatrix}^{\mathrm{T}}$ and $\mathrm{y}_{\mathrm{out}} = \mathrm{y}_2 = \begin{pmatrix} t_2 & \theta_2 \end{pmatrix}^{\mathrm{T}}$

Most likely path of protons

Bayesian formalism

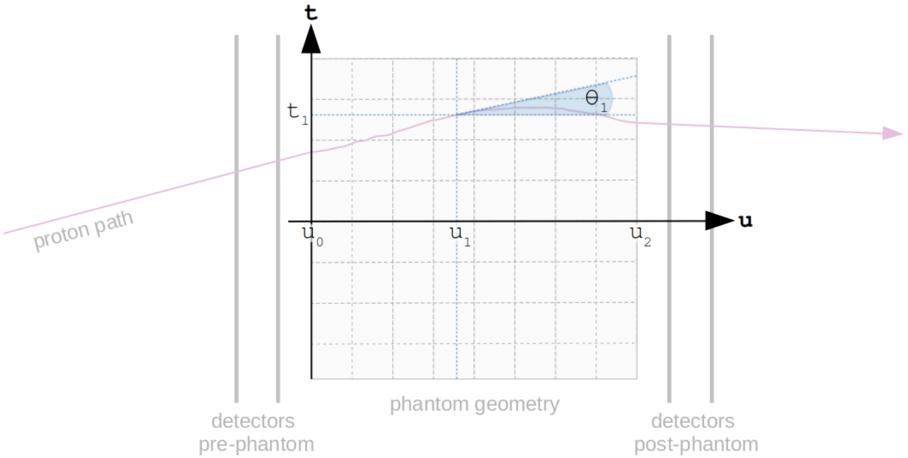

Most likely path of protons

Bayesian formalism

- The MLP is calculated by Equation (24) in [Schulte et al., 2008];

$$y_{\mathrm{MLP}} = \left(\Sigma_1^{-1} + R_1^T \Sigma_2^{-1} R_1\right)^{-1} \left(\Sigma_1^{-1} R_0 y_0 + R_1^T \Sigma_2^{-1} y_2\right) \tag{4}$$

Most likely path of protons

Bayesian formalism

- The MLP is calculated by Equation (24) in [Schulte et al., 2008];

$$y_{\mathrm{MLP}} = \left(\Sigma_1^{-1} + R_1^T \Sigma_2^{-1} R_1\right)^{-1} \left(\Sigma_1^{-1} R_0 y_0 + R_1^T \Sigma_2^{-1} y_2\right) \quad (4)$$

- R_0 and R_1 are change-of-basis matrices,

$$R_0 = \begin{pmatrix} 1 & u_1 - u_0 \\ 0 & 1 \end{pmatrix}, \quad R_1 = \begin{pmatrix} 1 & u_2 - u_1 \\ 0 & 1 \end{pmatrix} \quad (5)$$

Most likely path of protons

Bayesian formalism

- The MLP is calculated by Equation (24) in [Schulte et al., 2008];

$$y_{\mathrm{MLP}} = \left(\Sigma_1^{-1} + R_1^T \Sigma_2^{-1} R_1\right)^{-1} \left(\Sigma_1^{-1} R_0 y_0 + R_1^T \Sigma_2^{-1} y_2\right) \tag{4}$$

- R_0 and R_1 are change-of-basis matrices,

$$R_0 = \begin{pmatrix} 1 & u_1 - u_0 \\ 0 & 1 \end{pmatrix}, \quad R_1 = \begin{pmatrix} 1 & u_2 - u_1 \\ 0 & 1 \end{pmatrix} \tag{5}$$

- Σ_1 and Σ_2 are the covariance matrices,

$$\Sigma_1 = \begin{pmatrix} \sigma^2_{t_1} & \sigma^2_{t_1\theta_1} \\ \sigma^2_{t_1\theta_1} & \sigma^2_{\theta_1} \end{pmatrix}, \quad \Sigma_2 = \begin{pmatrix} \sigma^2_{t_2} & \sigma^2_{t_2\theta_2} \\ \sigma^2_{t_2\theta_2} & \sigma^2_{\theta_2} \end{pmatrix} \tag{6}$$

Most likely path of protons

Bayesian formalism

Definition

Scattering power: the rate of increase, with depth u, of the mean square of the projected scattering angle θ;

$$T(u) \equiv \frac{d\langle\theta^2\rangle}{du}. \tag{7}$$

Most likely path of protons

Bayesian formalism

Definition

Scattering power: the rate of increase, with depth u, of the mean square of the projected scattering angle θ;

$$T(u) \equiv \frac{d\langle\theta^2\rangle}{du}. \tag{7}$$

- Elements of the covariance matrices in (6), known as *scattering moments*, given by (for $i = 1, 2$)

$$\sigma^2_{\theta_i} \equiv A_0(u_i) = \int_{u_{i-1}}^{u_i} T(\eta)d\eta, \tag{8}$$

$$\sigma^2_{t_i\theta_i} \equiv A_1(u_i) = \int_{u_{i-1}}^{u_i} (u_i - \eta)T(\eta)d\eta, \tag{9}$$

$$\sigma^2_{t_i} \equiv A_2(u_i) = \int_{u_{i-1}}^{u_i} (u_i - \eta)^2 T(\eta)d\eta, \tag{10}$$

Most likely path of protons

Bayesian formalism

- The variance in lateral displacement is given by the (1,1) matrix element of (11) [Schulte et al., 2008];

$$\epsilon_{t_1\theta_1} = 2\left(\Sigma_1^{-1} + R_1^T \Sigma_2^{-1} R_1\right)^{-1}. \tag{11}$$

Most likely path of protons

Bayesian formalism

- The variance in lateral displacement is given by the (1,1) matrix element of (11) [Schulte et al., 2008];

$$\epsilon_{t_1\theta_1} = 2\left(\Sigma_1^{-1} + R_1^T \Sigma_2^{-1} R_1\right)^{-1}. \tag{11}$$

- This error matrix may be used to define a probability envelope surrounding the most likely path.

Inhomogeneous MLP formalism

Calculation of scattering moments

- Gottschalk's method [Gottschalk, 2010] has been used to approximate the scattering power $T(u)$ at depth u as

$$T(u) = \frac{2\pi}{\alpha}\left(m_e c^2\right)^2 \left(\frac{\tau+1}{\tau+2}\right)^2 \frac{1}{E^2(u)}\frac{1}{X_s} \tag{12}$$

Inhomogeneous MLP formalism

Calculation of scattering moments

- Gottschalk's method [Gottschalk, 2010] has been used to approximate the scattering power $T(u)$ at depth u as

$$T(u) = \frac{2\pi}{\alpha}\left(m_e c^2\right)^2 \left(\frac{\tau+1}{\tau+2}\right)^2 \frac{1}{E^2(u)} \frac{1}{X_s} \tag{12}$$

- $E(u)$ is the depth-dependent kinetic energy of the proton

Inhomogeneous MLP formalism

Calculation of scattering moments

- Gottschalk's method [Gottschalk, 2010] has been used to approximate the scattering power $T(u)$ at depth u as

$$T(u) = \frac{2\pi}{\alpha}\left(m_e c^2\right)^2 \left(\frac{\tau+1}{\tau+2}\right)^2 \frac{1}{E^2(u)}\frac{1}{X_s} \tag{12}$$

- $E(u)$ is the depth-dependent kinetic energy of the proton
- $\tau = E(u)/m_p c^2$ is the *reduced kinetic energy* of the proton

Inhomogeneous MLP formalism

Calculation of scattering moments

- Gottschalk's method [Gottschalk, 2010] has been used to approximate the scattering power $T(u)$ at depth u as

$$T(u) = \frac{2\pi}{\alpha}\left(m_e c^2\right)^2 \left(\frac{\tau+1}{\tau+2}\right)^2 \frac{1}{E^2(u)} \frac{1}{X_s} \tag{12}$$

- $E(u)$ is the depth-dependent kinetic energy of the proton
- $\tau = E(u)/m_p c^2$ is the *reduced kinetic energy* of the proton
- Gottschalk introduced the *scattering length* $1/X_s$, given by

$$\frac{1}{X_s} \equiv \alpha N_A \rho \left(\frac{e^2}{m_e c^2}\right)^2 \frac{Z}{A}\left\{2\ln\left[33219(AZ)^{-1/3}\right] - 1\right\} \tag{13}$$

where ρ is the mass density.

Inhomogeneous MLP formalism

Calculation of scattering moments

- If the composite material consists of n elements, each with fractional weight per volume $0 < w_k \leq 1, k = 1, \ldots, n$ then

$$\frac{1}{X_s} = \rho \sum_{k=1}^{n} w_k \left(\frac{1}{\rho X_s} \right)_k \tag{14}$$

where ρ is the density of the composite material.

Inhomogeneous MLP formalism

Calculation of scattering moments

- If the composite material consists of n elements, each with fractional weight per volume $0 < w_k \leq 1, k = 1, \ldots, n$ then

$$\frac{1}{X_s} = \rho \sum_{k=1}^{n} w_k \left(\frac{1}{\rho X_s} \right)_k \tag{14}$$

where ρ is the density of the composite material.

Inhomogeneous MLP formalism

Calculation of scattering moments

- If the composite material consists of n elements, each with fractional weight per volume $0 < w_k \leq 1, k = 1, \ldots, n$ then

$$\frac{1}{X_s} = \rho \sum_{k=1}^{n} w_k \left(\frac{1}{\rho X_s} \right)_k \tag{14}$$

where ρ is the density of the composite material.

Definition

Relative scattering power (RScP): the ratio of the scattering power in the material of interest to that in water;

$$\mathrm{RScP} \equiv \hat{T} = \frac{T}{T_{\mathrm{w}}}. \tag{15}$$

Inhomogeneous MLP formalism

Calculation of scattering moments

- RScP is simply the ratio of scattering lengths and is thus energy independent.

Inhomogeneous MLP formalism

Calculation of scattering moments

- RScP is simply the ratio of scattering lengths and is thus energy independent.

- It can be shown that

$$\hat{T} = \frac{\rho}{\rho_\mathrm{w}} \frac{ZA_\mathrm{w}}{Z_\mathrm{w}A} \left[\frac{19.8218 - \frac{2}{3}\ln(ZA)}{19.8218 - \frac{2}{3}\ln(Z_\mathrm{w}A_\mathrm{w})} \right] \tag{16}$$

where the subscript 'w' refers to the value for water.

Inhomogeneous MLP formalism

Calculation of scattering moments

- RScP is simply the ratio of scattering lengths and is thus energy independent.
- It can be shown that

$$\hat{T} = \frac{\rho}{\rho_{\mathrm{w}}} \frac{ZA_{\mathrm{w}}}{Z_{\mathrm{w}}A} \left[\frac{19.8218 - \frac{2}{3}\ln(ZA)}{19.8218 - \frac{2}{3}\ln(Z_{\mathrm{w}}A_{\mathrm{w}})} \right] \tag{16}$$

where the subscript 'w' refers to the value for water.

- We can now calculate the scattering power at any depth u using

$$T(u) = T_{\mathrm{w}}(u)\hat{T}. \tag{17}$$

Inhomogeneous MLP formalism

Calculation of scattering moments

- $T_{\mathrm{w}}(u)$ requires the kinetic energy of the proton to be known at depth u

Inhomogeneous MLP formalism

Calculation of scattering moments

- $T_{\mathrm{w}}(u)$ requires the kinetic energy of the proton to be known at depth u
- Use definition of stopping power and RStP to estimate the kinetic energy

 mark.brooke@oncology.ox.ac.uk @markdanbrooke

Inhomogeneous MLP formalism

Calculation of scattering moments

- $T_{\mathrm{w}}(u)$ requires the kinetic energy of the proton to be known at depth u
- Use definition of stopping power and RStP to estimate the kinetic energy
- Forward Euler method:

$$E_j^F = E_{j-1}^F - \hat{S}_j S_{\mathrm{w}}(E_j^F)\delta u, \quad j = 1, \ldots, N, \tag{18}$$

Inhomogeneous MLP formalism

Calculation of scattering moments

- $T_{\mathrm{w}}(u)$ requires the kinetic energy of the proton to be known at depth u
- Use definition of stopping power and RStP to estimate the kinetic energy
- Forward Euler method:

$$E_j^F = E_{j-1}^F - \hat{S}_j S_{\mathrm{w}}(E_j^F)\delta u, \quad j = 1, \ldots, N, \tag{18}$$

- Backward Euler method:

$$E_j^B = E_{j+1}^B + \hat{S}_j S_{\mathrm{w}}(E_{j+1}^B)\delta u, \quad j = 0, \ldots, N-1 \tag{19}$$

Inhomogeneous MLP formalism

Calculation of scattering moments

- $T_{\mathrm{w}}(u)$ requires the kinetic energy of the proton to be known at depth u
- Use definition of stopping power and RStP to estimate the kinetic energy
- Forward Euler method:

$$E_j^F = E_{j-1}^F - \hat{S}_j S_{\mathrm{w}}(E_j^F)\delta u, \quad j = 1, \dots, N, \tag{18}$$

- Backward Euler method:

$$E_j^B = E_{j+1}^B + \hat{S}_j S_{\mathrm{w}}(E_{j+1}^B)\delta u, \quad j = 0, \dots, N-1 \tag{19}$$

- $\hat{S}_j$ is the RStP at discrete depth u_j

Inhomogeneous MLP formalism

Calculation of scattering moments

- Stopping powers in water can be determined using the Bethe-Bloch formula,

$$S(E) \equiv -\left\langle \frac{dE}{du} \right\rangle = \frac{4\pi}{m_e c^2} \frac{\rho_e}{\beta^2} \left(\frac{e^2}{4\pi\epsilon_0} \right)^2 \left[\ln \left(\frac{2 m_e c^2 \beta^2}{I(1-\beta^2)} \right) - \beta^2 \right] \quad (20)$$

Inhomogeneous MLP formalism

Calculation of scattering moments

- Stopping powers in water can be determined using the Bethe-Bloch formula,

$$S(E) \equiv -\left\langle \frac{dE}{du} \right\rangle = \frac{4\pi}{m_e c^2} \frac{\rho_e}{\beta^2} \left(\frac{e^2}{4\pi\epsilon_0} \right)^2 \left[\ln\left(\frac{2 m_e c^2 \beta^2}{I(1-\beta^2)} \right) - \beta^2 \right] \tag{20}$$

- ρ_e is the electron number density of the material and I is the *mean excitation potential*

Inhomogeneous MLP formalism

Calculation of scattering moments

- Stopping powers in water can be determined using the Bethe-Bloch formula,

$$S(E) \equiv -\left\langle \frac{dE}{du} \right\rangle = \frac{4\pi}{m_e c^2} \frac{\rho_e}{\beta^2} \left(\frac{e^2}{4\pi\epsilon_0} \right)^2 \left[\ln\left(\frac{2 m_e c^2 \beta^2}{I(1-\beta^2)} \right) - \beta^2 \right] \tag{20}$$

- ρ_e is the electron number density of the material and I is the *mean excitation potential*
- Experimental values of the mean excitation potential for a single-element substance (e.g. O_2 gas) can be looked up in a database

Inhomogeneous MLP formalism

Calculation of scattering moments

- RStP exhibits negligible energy dependence in the range of 3 to 300 MeV for the materials investigated

Inhomogeneous MLP formalism

Calculation of scattering moments

- RStP exhibits negligible energy dependence in the range of 3 to 300 MeV for the materials investigated
- We can now calculate the stopping power at any depth u using

$$S(u) = S_{\mathrm{w}}(u)\hat{S}. \tag{21}$$

Inhomogeneous MLP formalism

Calculation of scattering moments

- RStP exhibits negligible energy dependence in the range of 3 to 300 MeV for the materials investigated
- We can now calculate the stopping power at any depth u using

$$S(u) = S_{\mathrm{w}}(u)\hat{S}. \tag{21}$$

- In the proposed use of this method, the current estimate of RSP from the reconstructed image will be used to update RSP in each voxel.

Inhomogeneous MLP formalism

MLP-spline-hybrid method

- Wish to increase computational efficiency

Inhomogeneous MLP formalism

MLP-spline-hybrid method

- Wish to increase computational efficiency
- Inhomogeneous MLP (denoted MLP_{x}) may be calculated only at material boundaries in a heterogeneous phantom

Inhomogeneous MLP formalism

MLP-spline-hybrid method

- Wish to increase computational efficiency
- Inhomogeneous MLP (denoted MLP_{x}) may be calculated only at material boundaries in a heterogeneous phantom
- Entire trajectory is then estimated by fitting a cubic spline through the boundary data, given the initial and final directions of the proton

Inhomogeneous MLP formalism

MLP-spline-hybrid method

- Wish to increase computational efficiency
- Inhomogeneous MLP (denoted MLP_{x}) may be calculated only at material boundaries in a heterogeneous phantom
- Entire trajectory is then estimated by fitting a cubic spline through the boundary data, given the initial and final directions of the proton
- Denote this spline-hybrid approach $\mathrm{MLP}_{\mathrm{x}}\mathrm{SH}$

Catalogue of anatomical materials

ID	Material	$\hat{T}$	$\hat{S}$	$\sigma_{\hat{S}}$ ($\times 10^{-2}$)	ID	Material	$\hat{T}$	$\hat{S}$	$\sigma_{\hat{S}}$ ($\times 10^{-2}$)
1	Adipose Child #1	0.89504	0.98819	0.080	25	Ovary	1.03668	1.04422	0.009
2	Adipose Child #2	0.85245	0.96906	0.103	26	Pancreas	1.00525	1.03704	0.014
3	Adipose Child #3	0.81864	0.96224	0.131	27	Skin Adult	1.04607	1.07811	0.003
4	Adipose Adult #1	0.84351	0.97922	0.119	28	Spleen Adult	1.04356	1.05000	0.012
5	Adipose Adult #2	0.80589	0.96295	0.140	29	Testis	1.02414	1.03567	0.003
6	Adipose Adult #3	0.76853	0.94665	0.162	30	Thyroid	1.03159	1.04147	0.006
7	Lipoma	0.80313	0.99125	0.158	31	Urinary Bladder (Empty)	1.02807	1.03220	0.010
8	Blood Adult	1.04510	1.04967	0.016	32	Water	1	1	0
9	Brain Adult	1.01573	1.03654	0.008	33	Skeleton Yellow Marrow	0.81917	0.99433	0.159
10	Breast Mammary Gland #1	0.86546	0.99639	0.108	34	Skeleton Red Marrow	0.93235	1.02952	0.072
11	Breast Mammary Gland #2	0.93908	1.01948	0.058	35	Skeleton Cartilage Adult	1.11620	1.07817	0.073
12	Breast Mammary Gland #3	1.02495	1.05108	0.002	36	Skeleton Cortical Bone Adult	2.72651	1.69534	1.114
13	Breast Whole (50/50)	0.86365	0.97171	0.099	37	Skeleton Cranium	2.10373	1.46368	0.703
14	Breast Whole (33/67)	0.81350	0.95312	0.130	38	Skeleton Femur Adult (30 yrs)	1.55809	1.25184	0.344
15	Eye Lens	1.02782	1.05615	0.010	39	Skeleton Femur Adult (90 yrs)	1.35430	1.16568	0.219
16	GI Tract	1.00727	1.02423	0.004	40	Skeleton Humerus	1.79596	1.35091	0.496
17	Heart Adult (Healthy)	1.02557	1.04185	0.001	41	Skeleton Mandible	2.23854	1.51680	0.790
18	Heart Adult (Fatty)	1.00500	1.03341	0.006	42	Skeleton Ribs (2nd, 6th)	1.69826	1.31384	0.433
19	Kidney Adult	1.02861	1.04136	0.007	43	Skeleton Ribs (10th)	1.91900	1.39837	0.579
20	Liver Adult (Healthy)	1.03899	1.05002	0.011	44	Skeleton Sacrum Male	1.45649	1.22427	0.275
21	Liver Adult (Fatty)	1.01532	1.04229	0.005	45	Skeleton Spongiosa	1.24427	1.13916	0.136
22	Lung Adult (Healthy)	0.25659	0.25781	0.004	46	Skeleton Vertebral Column C4	1.71726	1.32177	0.447
23	Lymph	1.02702	1.02319	0.010	47	Air	0.00121	0.00108	< 0.001
24	Muscle Skeletal Adult	1.02672	1.04130	0.008					

Catalogue of anatomical materials

- RScP ($\hat{T}$) and RStP ($\hat{S}$) values have bee calculated for human tissues listed in ICRU Report 46 [White et al., 1992] (and air)

Catalogue of anatomical materials

- RScP ($\hat{T}$) and RStP ($\hat{S}$) values have bee calculated for human tissues listed in ICRU Report 46 [White et al., 1992] (and air)
- Each material is given an identification (ID) number

Catalogue of anatomical materials

- RScP ($\hat{T}$) and RStP ($\hat{S}$) values have bee calculated for human tissues listed in ICRU Report 46 [White et al., 1992] (and air)
- Each material is given an identification (ID) number
- Any mean excitation values (I) used in the calculation of stopping power were obtained from ICRU Report 49 [Berger et al., 1993]

Relation between RStP and RScP

- In a pCT reconstruction algorithm, RStP in each voxel may be updated on successive iterations to build an image of the body

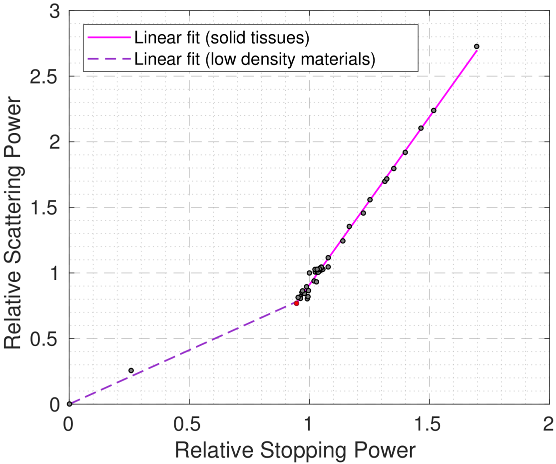

Relation between RStP and RScP

- In a pCT reconstruction algorithm, RStP in each voxel may be updated on successive iterations to build an image of the body
- Implementation of a calibration curve that determines RScP from RStP could provide an improvement to convergence of the algorithm and the final accuracy of the image

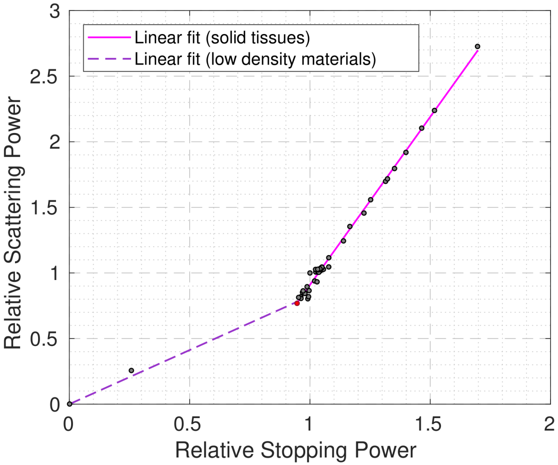

Metric for comparing MLP estimates

- We propose a metric G that assigns a single value to an MLP estimate, allowing for simple comparisons between different formalisms, geometries and beam characteristics.

$$G = \frac{1}{n_p} \sum_{i=1}^{n_p} \sum_{j=1}^{N} g_{ij} \tag{22}$$

Metric for comparing MLP estimates

- We propose a metric G that assigns a single value to an MLP estimate, allowing for simple comparisons between different formalisms, geometries and beam characteristics.

$$G = \frac{1}{n_p} \sum_{i=1}^{n_p} \sum_{j=1}^{N} g_{ij} \tag{22}$$

- n_p is the number of proton tracks used in the MLP calculation, N is the number of discrete depths at which a proton's lateral deviation t is recorded and

$$g_{ij} = \frac{\left| t_{i,\mathrm{mlp}}(u_j) - t_i(u_j) \right|^2}{\hat{\sigma}_t^2(u_j)}. \tag{23}$$

Metric for comparing MLP estimates

- We propose a metric G that assigns a single value to an MLP estimate, allowing for simple comparisons between different formalisms, geometries and beam characteristics.

$$G = \frac{1}{n_p} \sum_{i=1}^{n_p} \sum_{j=1}^{N} g_{ij} \tag{22}$$

- n_p is the number of proton tracks used in the MLP calculation, N is the number of discrete depths at which a proton's lateral deviation t is recorded and

$$g_{ij} = \frac{\left| t_{i,\mathrm{mlp}}(u_j) - t_i(u_j) \right|^2}{\hat{\sigma}_t^2(u_j)}. \tag{23}$$

- $\hat{\sigma}_t(u_j)$ is the standard deviation in the estimate of the lateral deflection at depth u_j, given by the square root of the (1,1) matrix element in (11).

Metric for comparing MLP estimates

G value	Accuracy of MLP
$G = 0$	perfect
$0 < G \leq 1$	good
$G > 1$	unsatisfactory
$G \gg 1$	poor

Monte Carlo simulations

Setup

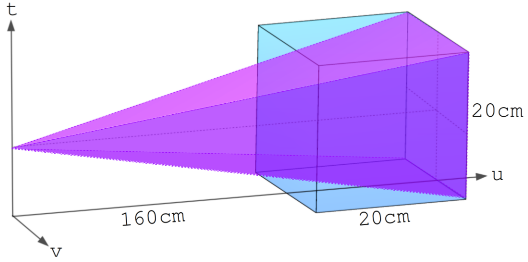

- An inhomogeneous geometry was created in *TOPAS* [Perl et al., 2012] consisting of water and thick slabs of cranium and cortical bone

Monte Carlo simulations
Setup

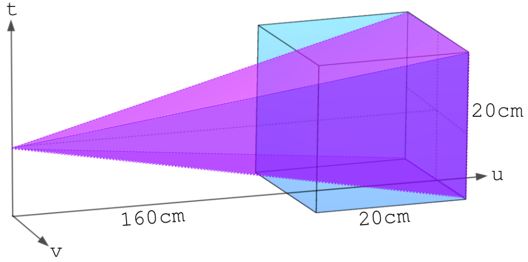

- An inhomogeneous geometry was created in *TOPAS* [Perl et al., 2012] consisting of water and thick slabs of cranium and cortical bone
- Proton histories were collected at 5 mm depth increments

Monte Carlo simulations
Setup

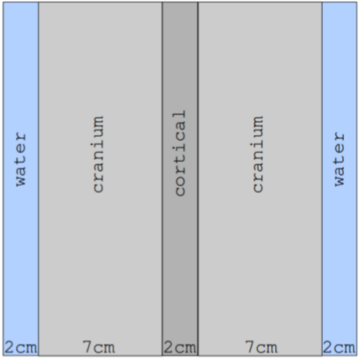

- Nominal beam energies of 230, 225, 220, 215 and 210 MeV were tested

Monte Carlo simulations

Results

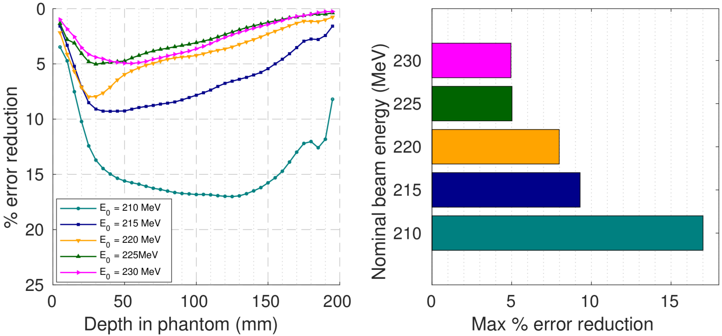

- Inhomogeneous formalism offers greatest accuracy improvement at lower energies, where scattering is more pronounced

Monte Carlo simulations

Results: 210 MeV protons

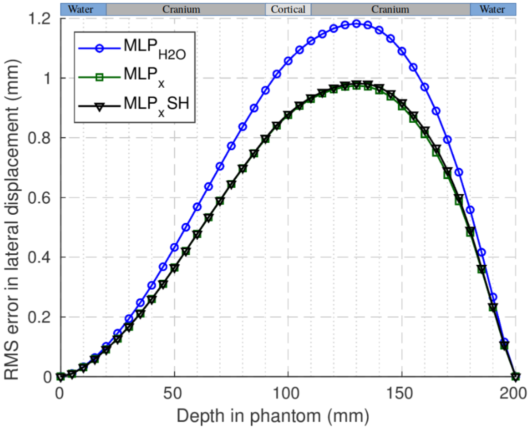

- Accounting for inhomogeneity (MLP_X) leads to approximately a 17% improvement in maximum RMS lateral position error when compared to the assumption of a water phantom (MLP_{H2O}) for a 210 MeV nominal beam energy

Monte Carlo simulations

Results: 210 MeV protons

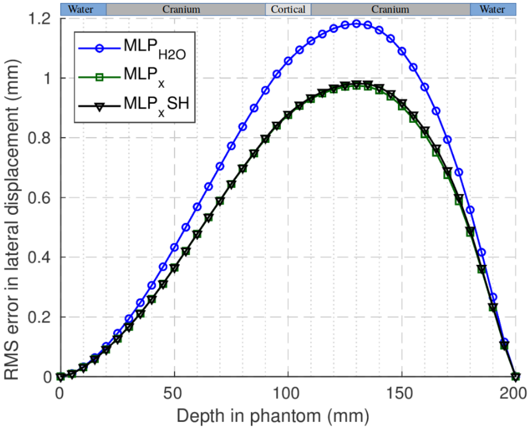

- Accounting for inhomogeneity (MLP_X) leads to approximately a 17% improvement in maximum RMS lateral position error when compared to the assumption of a water phantom (MLP_{H2O}) for a 210 MeV nominal beam energy
- Spline-Hybrid approach ($MLP_X SH$) achieved very similar results in 1/40th the time

Monte Carlo simulations

Results: 210 MeV protons

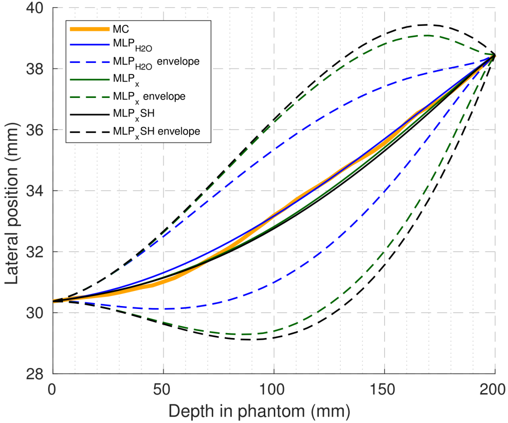

- Shape of probability envelope (skewness, width) depends on material

Monte Carlo simulations

Setup

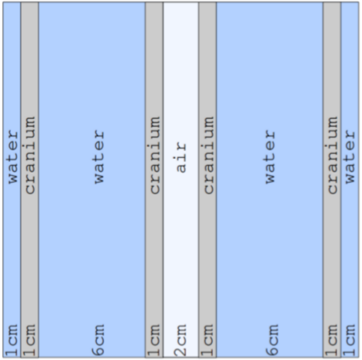

- More realistic geometry tested with a monoenergetic 190 MeV proton beam

Monte Carlo simulations

Results

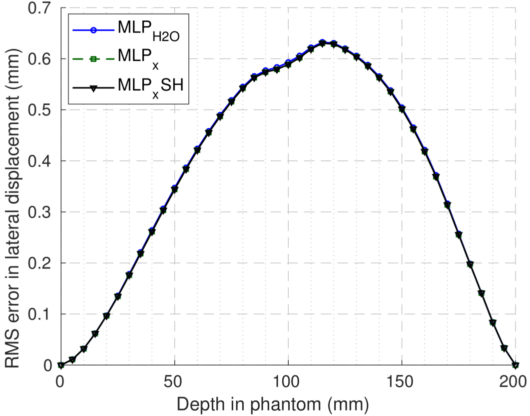

- No appreciable improvement in accuracy by employing inhomogeneous formalism

Monte Carlo simulations

Results

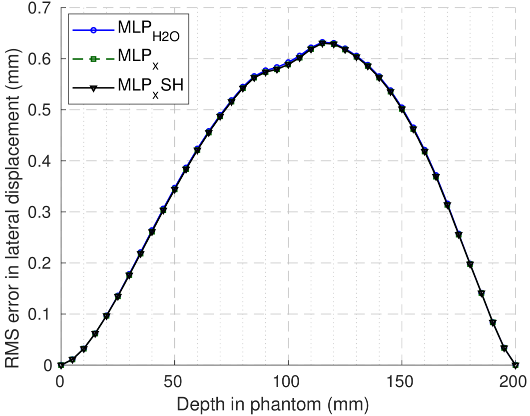

- No appreciable improvement in accuracy by employing inhomogeneous formalism
- Probability envelope is wider using the inhomogeneous formalism

Monte Carlo simulations

Results

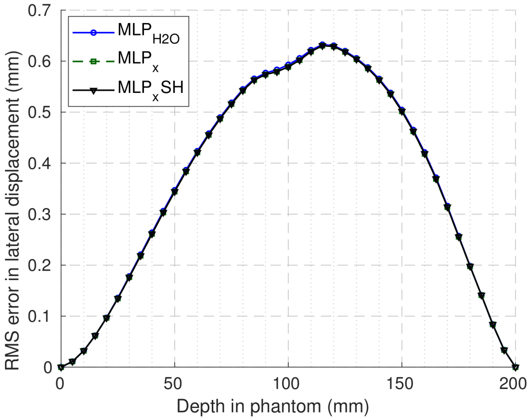

- No appreciable improvement in accuracy by employing inhomogeneous formalism
- Probability envelope is wider using the inhomogeneous formalism
- No appreciable improvement in accuracy by employing inhomogeneous formalism

Monte Carlo simulations

Results

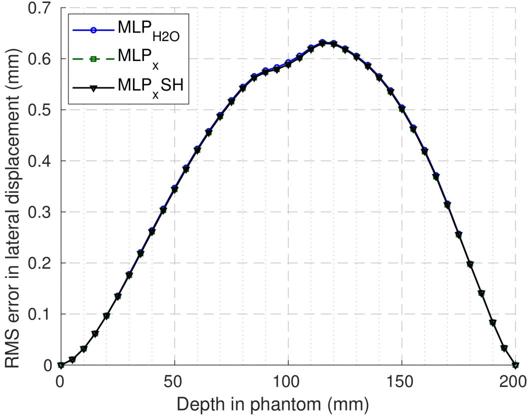

- No appreciable improvement in accuracy by employing inhomogeneous formalism
- Probability envelope is wider using the inhomogeneous formalism
- No appreciable improvement in accuracy by employing inhomogeneous formalism
- Probability envelope is wider using the inhomogeneous formalism

Results
Summary

		MLP_{H2O}		MLP_X		MLP_XSH	
		Metric value G	% tracks outside 3σ MLP envelope	Metric value G	% tracks outside 3σ MLP envelope	Metric value G	% tracks outside 3σ MLP envelope
Water Phantom (200 MeV)	No data cuts	1.65	7.57	1.42	7.27	1.48	6.57
	3σ cuts	0.633	3.07	0.585	2.50	0.581	1.93
	2σ cuts	0.564	2.04	0.520	1.57	0.514	1.07
Slab Phantom A	2σ cuts (210 MeV)	3.75	49.7	0.522	1.23	0.496	1.10
	2σ cuts (215 MeV)	1.95	24.2	0.526	1.33	0.524	1.17
	2σ cuts (220 MeV)	1.52	15.8	0.516	1.27	0.515	1.17
	2σ cuts (225 MeV)	1.33	11.1	0.523	1.50	0.520	1.23
	2σ cuts (230 MeV)	1.26	9.83	0.519	1.37	0.516	1.03
Slab Phantom B (190 MeV)	2σ cuts	0.608	1.80	0.504	1.35	0.490	1.20

Conclusions

- A catalogue of materials has been created based on RStP and RScP values

Conclusions

- A catalogue of materials has been created based on RStP and RScP values
- Bi-linear relationship shown between RStP an RScP which could be utilised in iterative pCT reconstruction

Conclusions

- A catalogue of materials has been created based on RStP and RScP values
- Bi-linear relationship shown between RStP an RScP which could be utilised in iterative pCT reconstruction
- Inhomogeneous formalism shows noticeable improvement in MLP accuracy for thick and dense materials, and at lower energies

Conclusions

- A catalogue of materials has been created based on RStP and RScP values
- Bi-linear relationship shown between RStP an RScP which could be utilised in iterative pCT reconstruction
- Inhomogeneous formalism shows noticeable improvement in MLP accuracy for thick and dense materials, and at lower energies
- Spline-Hybrid approach produces very similar results in a small fraction of the time

Conclusions

- A catalogue of materials has been created based on RStP and RScP values
- Bi-linear relationship shown between RStP an RScP which could be utilised in iterative pCT reconstruction
- Inhomogeneous formalism shows noticeable improvement in MLP accuracy for thick and dense materials, and at lower energies
- Spline-Hybrid approach produces very similar results in a small fraction of the time
- Probability envelope shape (skewness, width) depends on material

An inhomogeneous most likely path formalism for proton computed tomography

Mark Brooke, Scott Penfold

(Submitted on 1 Aug 2018)

Multiple Coulomb scattering (MCS) poses a challenge in proton CT (pCT) image reconstruction. The assumption of straight line paths is replaced with Bayesian models of the most likely path (MLP). Current MLP-based pCT reconstruction approaches assume a water scattering environment. In this work, an MLP formalism that takes into account the inhomogeneous composition of the human body has been proposed, which is based on the accurate determination of scattering moments in heterogeneous media. Monte Carlo simulation was used to compare the new inhomgeneous MLP formalism to the homogeneous water approach. An MLP-Spline-Hybrid method was investigated for improved computational efficiency and a metric was introduced for assessing the accuracy of the MLP estimate. Anatomical materials have been catalogued based on their relative stopping power (RStP) and relative scattering power (RScP) and a relationship between these two values was investigated. A bi-linear correlation between RStP and RScP is shown. When compared to Monte Carlo proton tracks through a 20 cm water cube with thick bone inserts using the TOPAS simulation toolkit, the inhomogeneous formalism was shown to predict proton paths to within 1.0 mm on average for beams ranging from 230 MeV down to 210 MeV incident energy. The improvement in accuracy over the conventional MLP approach from using the new formalism is most noticeable at lower energies, ranging from 5% for a 230 MeV beam to 17% for 210 MeV. Implementation of a new MLP-Spline-Hybrid method greatly reduced computation time while suffering negligible loss of accuracy. A more clinically relevant phantom was created by inserting thin slabs of bone and an air cavity into the water phantom. There was no noticeable gain in the accuracy of predicting 190 MeV Monte Carlo proton paths using the inhomogeneous formalism in this case.

Subjects: **Medical Physics (physics.med-ph)**

Cite as: arXiv:1808.00122 **[physics.med-ph]**

(or arXiv:1808.00122v1 **[physics.med-ph]** for this version)

Download:

- PDF
- Other formats

(license)

Current browse context:

physics.med-ph

< prev | next >

new | recent | 1808

Change to browse by:

physics

References & Citations

- NASA ADS

Bookmark (what is this?)

Acknowledgements

This project was commenced as an Honours thesis at the University of Adelaide, supervised by Dr. Scott Penfold. His ongoing support and contributions have been invaluable.

This work was supported by Cancer Research UK grant number C2195/A25197, through a CRUK Oxford Centre DPhil Prize Studentship.

DPhil supervisors: Prof. Frank Van den Heuvel, Prof. Maria Hawkins, Dr. Francesca Fiorini

Radiation Therapy Medical Physics Group: Prof. Frank Van den Heuvel, Dr. Francesca Fiorini, Dr. Suliana Teoh, Dr. Ben George, Mark Brooke.

Many thanks to the General Sir John Monash Foundation, Cancer Research UK and the Clarendon Fund for supporting my studies.

References

M. J. Berger, M. Inokuti, H. H. Andersen, H. Bichsel, D. Powers, S. . M. Seltzer, D. . Thwaites, and D. E. Watt. Report 49. *Journal of the ICRU*, os25(2):NP, 1993. doi: 10.1093/jicru/os25.2.Report49. URL http://jicru.oxfordjournals.org/content/os25/2/NP.short.

B. Gottschalk. On the scattering power of radiotherapy protons. *Medical Physics*, 37(1), 2010.

H. Jiang, J. Seco, and H. Paganetti. Effects of hounsfield number conversion on ct based proton monte carlo dose calculations. *Medical Physics*, 34 (4):1439–1449, 2007. ISSN 2473-4209. doi: 10.1118/1.2715481. URL http://dx.doi.org/10.1118/1.2715481.

J. Perl, J. Shin, J. Schumann, B. Faddegon, and H. Paganetti. TOPAS: An innovative proton Monte Carlo platform for research and clinical applications. *Medical Physics*, 39:6818, 2012. doi: 10.1118/1.4758060.

R. W. Schulte, S. N. Penfold, J. T. Tafas, and K. E. Schubert. A maximum likelihood proton path formalism for application in proton computed tomography. *Medical Physics*, 35(11):4849–4856, 2008. doi: http://dx.doi.org/10.1118/1.2986139. URL http://scitation.aip.org/content/aapm/journal/medphys/35/11/10.1118/1.2986139.

A. R. Smith. Vision 20/20: Proton therapy. *Medical Physics*, 36(2):556–568, 2009. ISSN 2473-4209. doi: 10.1118/1.3058485. URL http://dx.doi.org/10.1118/1.3058485.

D. R. White, R. V. Griffith, and I. J. Wilson. Report 46. *Journal of the ICRU*, os24(1):NP, 1992. doi: 10.1093/jicru/os24.1.Report46. URL http://jicru.oxfordjournals.org/content/os24/1/NP.short.

D. C. Williams. The most likely path of an energetic charged particle through a uniform medium. *Physics in Medicine and Biology*, 49(13):2899, 2004. URL http://stacks.iop.org/0031-9155/49/i=13/a=010.